

Thorium distribution on the Moon: new insights from *Chang'E-2* gamma-ray spectrometer^{*}

Meng-Hua Zhu^{1,2,3**}, Jin Chang² and Tao Ma²

¹ State Key Laboratory of Lunar and Planetary Sciences, Macau University of Science and Technology, Taipa, Macau, China; mhzhu@must.edu.mo

² Purple Mountain Observatory, Chinese Academy of Sciences, Nanjing 210034, China

³ CAS Center for Excellence in Comparative Planetology, Hefei 230026, China

Received 2018 September 18; accepted 2019 March 22

Abstract We present the thorium distribution on the lunar surface derived from observations by the *Chang'E-2* gamma-ray spectrometer (*CE-2* GRS). This new map shows a similar thorium distribution to previous observations. In combination with this new thorium map and impact cratering model, we investigate the origination of thorium on the Moon's highlands, which was previously thought to be contributed from Imbrium ejecta. We found that the Imbrium ejecta has a small contribution ($\sim 20\% - 30\%$) to the thorium on the lunar highlands but most thorium is likely to be indigenous before the deposition of the Imbrium ejecta. This new thorium map also confirms that the eastern highlands have a relatively higher thorium concentration than the western highlands. We propose that the thin crust and large basins on the eastern highlands are responsible for this difference in thorium.

Key words: Moon — *Chang'E-2* Gamma-ray Spectrometer — Thorium distribution

1 INTRODUCTION

Associated with the asymmetric features of elevation and crustal thickness between the Moon's nearside and far-side is the radioactive elemental distributions (Prettyman et al. 2006; Kobayashi et al. 2010, 2012; Yamashita et al. 2010; Zhu et al. 2013). The nearside of the Moon, with a thin crust and relatively flat surface that is dominated by volcanic maria, is enriched in radioactive elements (i.e., thorium (Th), potassium (K) and uranium (U)). The mountainous and rugged farside, characterized by heavily cratered feldspathic highlands with thick crust, is depleted in radioactive elements. These distinct geological differences imply a diverse evolutionary history from their initial stages to the current state. According to the Th and FeO concentrations on the lunar surface, Jolliff et al. (2000) divided the lunar surface into three major geological provinces: the Procellarum KREEP Terrane (PKT), the Feldspathic Highlands Terrane (FHT) and the South Pole-Aitken Terrane (SPAT). Within the PKT, the compo-

sitions are enriched in Th with a concentration larger than 3 ppm (based on a *Lunar Prospector* (LP) $5^\circ \times 5^\circ$ Th map, Lawrence et al. 1998). The SPAT has a Th concentration between 1.5 ppm and 3.5 ppm. In contrast, the FHT, constituting over 60% of the Moon's surface, is depleted of Th, with a concentration lower than 1.5 ppm.

The Th contained within the KREEP materials was thought to be last crystallized between the boundary of the crust and mantle during solidification of the lunar magma ocean (Warren 1985) due to the incompatibly large ionic radius for the major minerals constituting the lunar crust and mantle (Korotev 1998). Although the global distribution and small-area features of the Th distribution have been observed and discussed in previous literatures (e.g., Lawrence et al. 1998, 2000, 2003; Haskin 1998; Korotev 1998; Jolliff et al. 2000; Haskin et al. 2000), the geological processes for their emplacements on the lunar surface are still not well understood. For example, Wasson & Warren (1980) and Hess & Parmentier (2001) argued that the high Th concentration in the PKT may result from the asymmetric crystallization of lunar magma ocean with a thickened KREEP liquid layer; Jutzi & Asphaug (2011) suggested that the high KREEP within the PKT was probably due to the low-velocity impact ($\sim 2.4 \text{ km s}^{-1}$) from a companion

^{*} A contributed paper from the International Symposium on Lunar and Planetary Science (ISLPS) held on 2018 June 12–15 at Macau University of Science and Technology.

^{**} Corresponding author.

moon, which displaced the global KREEP-rich layer to the nearside.

In contrast to the extensive studies on the Th origination in the PKT and SPAT, little is known about the distribution and origination of the Th on the lunar highlands surface. The major reason is that the highlands have low Th concentration, which is difficult to measure accurately using a normal gamma-ray spectrometer (GRS). It requires a sensitive instrument with the abilities to detect low-abundance Th and identify tiny spatial variations. During the past few years, several spacecraft with significantly improved GRSs (Feldman et al. 1999; Ma et al. 2008; Hasebe et al. 2008; Ma et al. 2013) than those from the Apollo era have been sent into orbits around the Moon to collect valuable observations. *Chang'E-2* (*CE-2*), the second lunar probe built by China, was launched on 2010 October 1 and inserted into a circular polar orbit with altitude of 100 km on 2010 October 15. The *CE-2* spacecraft carried a GRS with a special design (Ma et al. 2013) that has a high efficiency for the detection of gamma rays emitted from the lunar surface and, therefore, provides an opportunity to investigate the Th emplacement on the lunar highlands.

2 THORIUM ON THE MOON

Gamma rays, emitted from the lunar surface, are produced from the decay of natural radioactive elements (for example, U, Th and K) and the excitation of major elements (for example, Fe, Ti, Mg, Al, Si, O and Ca) due to interactions with incident Galactic cosmic rays (GCRs) (Reedy et al. 1973). The identification of gamma rays from orbit allows for the remote characterization of the elemental composition on the lunar surface (e.g., Prettyman et al. 2006; Zhu et al. 2013). The abundances of related elements within the field of view of a spacecraft can be derived from the measured gamma-ray spectra according to an inversion procedure (see the details in Reedy et al. 1973; Lawrence et al. 2000; and Kobayashi et al. 2010).

2.1 *CE-2* GRS and Its Observations

The *CE-2* GRS used a large LaBr₃ crystal ($\varphi 10.8 \text{ cm} \times 7.8 \text{ cm}$) as the main detector to detect the gamma-ray photons within an energy region between 0.3 and 9 MeV (Ma et al. 2013). Its has an energy resolution of $\sim 5\%$ full width at half maximum (FWHM) at 662 keV, which is higher than previous scintillator GRSs (e.g., *LP* and *Chang'E-1*) that were used to detect the compositional distribution on the lunar surface (Feldman et al. 1999; Zhu et al. 2010). Gamma rays entering into the main detector were accumulated within 3 s and then transferred to a spectrum with 512 channels. As the *CE-2* GRS was mounted inside the

spacecraft, a well-shaped CsI (Tl) crystal with a size of $\varphi 17.8 \text{ cm} \times 10.8 \text{ cm}$ was considered in anticoincidence with the main detector to suppress signal from the Compton effect and reduce the background gamma rays coming from GCRs interacting with the materials in the spacecraft (see the details of *CE-2* GRS in Ma et al. 2013).

The *CE-2* GRS had three period of observations. The first period of observation was in the cruise period from Earth to the Moon, during which *CE-2* GRS conducted about 80 hours of observations. All these observations were used to calibrate the instrument and estimate the self-background of the GRS and spacecraft. While the spacecraft entered into a circular polar-orbit with an altitude of 100 km from the Moon, the *CE-2* GRS recorded $\sim 178 \text{ d}$ of observations. After six months in lunar orbit, the *CE-2* departed to the Sun-Earth L2 point with the aim to investigate GCR variations in interplanetary space. The data used in this work were from observations during the cruise period and in lunar orbit.

The average gamma-ray spectrum for the whole Moon is shown in Figure 1(a), from which the energy peaks corresponding to elements on the Moon can be identified. However, due to limitations related to the purity of the LaBr₃ crystal, a gamma-ray spectrum with energy lower than 2.70 MeV is mainly dominated by self-activities from the LaBr₃ detector (Kernan 2006). For example, the spectrum below 1.7 MeV is primarily dominated by the natural decay of ¹³⁸La and that in 1.70 MeV and 2.70 MeV is dominated by the ²²⁷Ac decay chain generating alpha emitters. Due to the complicated background and non-Gaussian spectral shapes within the energy region of 1.70–2.70 MeV, in which the ²³²Th gamma-ray line at 2.61 MeV is located, it is difficult to resolve the net Th signal emitted from the lunar surface by using the peak fitting method. Alternatively, we use the energy band technique between 2.50 MeV and 2.71 MeV to determine the peak area for the spectra observed within the cruise period and in lunar orbit, respectively (Figs. 1(b)–(c)). We assume that gamma rays emitted from the decay of the LaBr₃ self-activity are constant during the whole mission and their contribution can be estimated from spectra in the cruise period. The net ²³²Th gamma rays (2.61 MeV) emanating from the lunar surface can be obtained by calculating the difference in the peak area between the lunar and cruise spectra. It should be noted that the peak area for ²³²Th in the lunar and cruise spectra are calculated from 2.50 MeV to 2.71 MeV to avoid unresolved contributions at the high-energy region around 2.75 MeV of Al originating from the lunar surface as well as the detector canister.

The spatial resolution on the lunar surface for an uncollimated, omnidirectional GRS, like the *CE-2* GRS, is a two-dimensional Gaussian function with an FWHM of

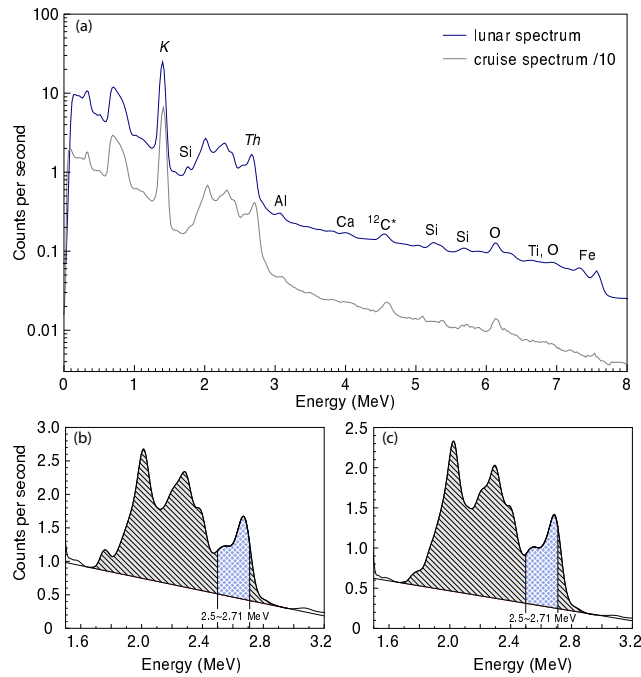


Fig. 1 *CE-2* gamma-ray spectrum plotted as counts per second versus energy from its 178 days of observations at an altitude of 100 km above the Moon and during the cruise period (a). The spectrum below 2.7 MeV is mainly contributed by self-activities from the LaBr_3 crystal: natural ^{138}La is primarily responsible for the spectrum below 1.7 MeV and the ^{227}Ac decay chain generates alpha emitters between 1.7 and 2.7 MeV, in which the Th line (2.64 MeV) is located. The spectral area of the orbital (b) and cruise spectrum (c) was calculated by using the energy band method between 2.50–2.71 MeV.

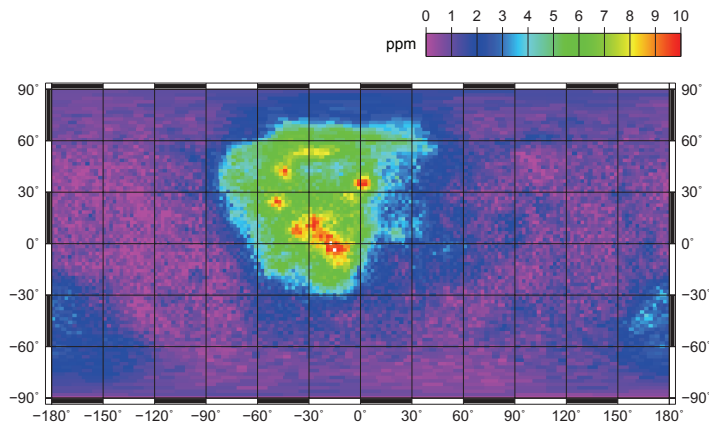


Fig. 2 The global Th distribution on the Moon derived from *CE-2* GRS. The Th gamma rays emitted from the Moon are binned into pixels of $60\text{ km} \times 60\text{ km}$ quasi-equal area (11 306 pixels). The map is displayed in cylindrical equidistant projection.

~ 1.5 times the height above the lunar surface (Reedy et al. 1973). For a normal observation at a 100-km working orbit above the Moon, the *CE-2* GRS can resolve the compositional variations on the lunar surface within an area of $150\text{ km} \times 150\text{ km}$. Nevertheless, to find the details of compositional variation within the spatial resolution (e.g., $150\text{ km} \times 150\text{ km}$), we re-binned all the spectra into the pixels on the Moon with an equal-area of about $60\text{ km} \times 60\text{ km}$ after the gain, solid angle and cosmic-ray-variation corrections. The detection efficiency of *CE-2*

GRS for the gamma rays at 2.61 MeV was estimated using the Monte Carlo method from 0° (sub-satellite point) to 70° (limited incident angle) with an increase interval of 0.5° . For each direction, we used a monochromatic beam with 9 000 000 gamma rays to estimate the energy deposited between 2.50 MeV and 2.71 MeV (with energy broadening). The measured gamma-ray flux was transferred to the flux of surface gamma rays at 2.61 MeV with a coefficient of 18.14 based on the spherical geometric relation (see Lawrence et al. 2000). The Th abundance in each

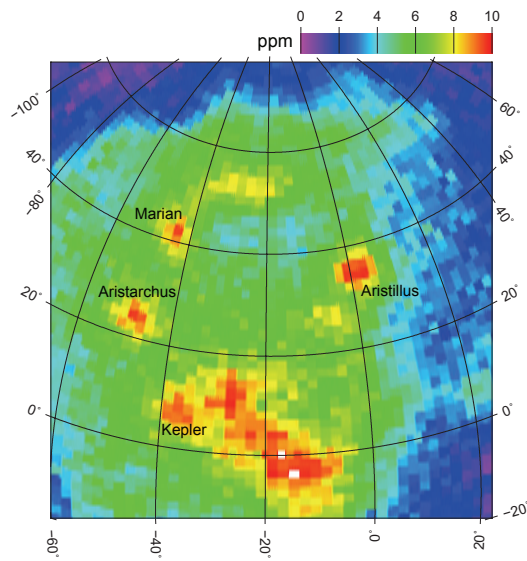


Fig. 3 The Th distribution in the PKT derived from *CE-2* GRS. The Th gamma rays emitted from the Moon are binned into pixels of $60 \text{ km} \times 60 \text{ km}$ quasi-equal area (11 306 pixels). The map is displayed in azimuthal projection.

pixel was determined by comparing the calculated gamma-ray flux to the emission rate of Th gamma rays at 2.61 MeV (see the details from Reedy et al. 1973; Lawrence et al. 2000).

2.2 The New Thorium Map on the Moon

The absolute Th map derived from the observations of *CE-2* GRS is shown in Figure 2. This new map has a similar distribution on the lunar surface as measurements from the *LP* (Lawrence et al. 2000; Prettyman et al. 2006) and *Kaguya* missions (Kobayashi et al. 2012). The high Th ($> 3.5 \text{ ppm}$) is mainly concentrated in the PKT. In contrast, the Th concentrations are relatively low in SPAT and FHT. In the PKT, the regions with high-Th concentration are located surrounding the Imbrium basin. These regions were thought to be associated with the Imbrium impact event (Haskin 1998; Lawrence et al. 2000). For example, four prominent high-Th craters (i.e., Aristarchus (25°N , 48°W), Marian (41°N , 43°W), Kepler (7°N , 38°W), and Aristillus (33°N , 3°E), see Fig. 3), which were thought to penetrate through the $\sim 2\text{-km}$ -thick mare basalt layer (Thomson et al. 2009) and expose the underlying high-Th materials (Lawrence et al. 2000), are located within the ejecta blanket of the Imbrium basin. The high-Th highlands in the north of Imbrium basin, extending from the rim of Sinus Iridum to Plato crater, were considered to be the rim of Imbrium basin. Another high-Th highland region in the southern part of PKT, covering the area between the west of Fra Mauro (5°S , 10°W) and the Carpathian Mountains (15°N , 30°W), was considered the ejecta from

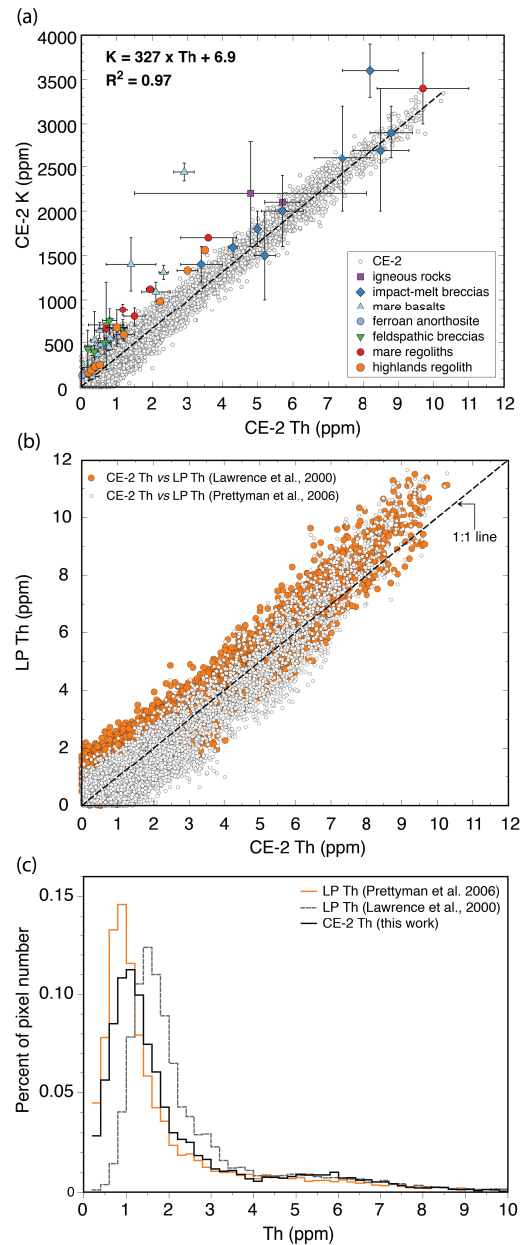


Fig. 4 The K/Th ratio from *CE-2* GRS and sample data (a). The comparison of Th abundance between *LP* GRS (Lawrence et al. 2000; Prettyman et al. 2006) and *CE-2* GRS (b). The comparison of Th histogram between *CE-2* and *LP* GRS (c). *LP* GRS Th map derived from 100 km-altitude observations (Lawrence et al. 2000; Prettyman et al. 2006) was used to avoid the abundance deviations caused by observation altitude.

Imbrium basin (Wilhelms et al. 1987). The presence of these high-Th regions is directly related to the high-Th Imbrium target before the impact event ~ 3.85 billion years ago (Stöffler & Ryder 2001).

Within the SPAT, the average Th concentration is $\sim 2.5 \text{ ppm}$, similar to previous observations (Lawrence et al. 2000; Kobayashi et al. 2012; Prettyman et al. 2006). A region with a relatively high Th concentration

(~ 3.5 ppm) is located at the northwest of the SPA basin, near the Ingenii basin (33.7°S , 163.5°E). The formation of this area with an anomalously high Th concentration is under debate. Garrick-Bethell & Zuber (2009) considered that the anomalous Th abundance within this area was from the excavation of the South Pole-Aitken (SPA) basin, whereas Wieczorek & Zuber (2001) and Haskin (1998) assumed that this anomalous Th abundance was the ejecta antipodal effect of the Serenitatis or Imbrium basin.

On the highlands of the Moon, most areas have low Th concentration, in agreement with previous observations (Lawrence et al. 2000; Kobayashi et al. 2012; Prettyman et al. 2006). An apparent region with a size of 150–300 km, located at the northern highlands between the Compton (55°N , 105°E) and Belkovich (60°N , 100°E) craters, has a relatively high Th concentration of 2–4 ppm. This anomalously high-Th region has a number of silicic volcanic characteristics (Jolliff et al. 2011) that are unusual over the lunar surface. The average Th concentration in the west-farside is ~ 1.1 ppm, whereas the average Th concentration of the east-farside is ~ 0.7 ppm. This small Th difference on the highlands between the west-farside and the east-farside was previously observed by the *LP* (Lawrence et al. 2000) and *Kaguya* GRSs (Kobayashi et al. 2012).

Lawrence et al. (2000) indicated that Poisson statistics (counting time and photon statistics) is similar to the measured uncertainties and dominates the abundance uncertainties in the low-Th pixels (see Lawrence et al. 2000 for the details). In this work, the largest uncertainty due to Poisson statistics for a $60\text{ km} \times 60\text{ km}$ pixel is 0.2 ppm. It means that the measured uncertainties are < 0.2 ppm in most low-Th pixels, therefore, the derived Th map can be confidently used for the investigation of Th emplacements on the lunar highlands surface.

Scatterplots of the Th and K (Zhu et al. 2013) abundances determined by *CE-2* GRS are shown in Figure 4(a), from which we can find the data are highly correlated. The K/Th ratio has a linear trend, similar to measurements from the *LP* observation (Prettyman et al. 2006). We also find that the K/Th ratio derived from *CE-2* GRS is consistent with the sample data (Korotev 1998) for the Th abundance > 4 ppm. However, for the Th abundance < 4 ppm, the K/Th ratio deviates a little from the sample data. We compare the Th abundances determined by *CE-2* GRS and *LP* GRS as well (see Fig. 4(b)). To avoid deviations in the abundance resulting from variations in the altitude at which the observations were acquired (Lawrence et al. 2003), we used the *LP* GRS Th map derived from the high-altitude observation ($\sim 100\text{ km}$ Lawrence et al. 2000; Prettyman et al. 2006). From Figure 4(b), we find that the Th abundance derived

from the *CE-2* GRS has a high correlation with that of *LP* GRS. Although both maps show a similar range in terms of Th concentrations on the Moon, the correlation exhibits a slight deviation from the 1:1 line. Comparing with the *LP* GRS Th map calculated from Prettyman et al. (2006), the *CE-2* Th map displays a lower value in the high range (~ 7 – 10 ppm) but a high value in the lower range (< 4 ppm). In contrast, the *LP* GRS Th abundance calculated from Lawrence et al. (2000) manifests a similar distribution with *CE-2* Th abundance at the low range. This difference can be identified by histograms of the percentage of the Th distribution on the Moon as well (see Fig. 4(c)). Although the percentages of Th distribution in PKT and SPAT are broadly similar to the maps derived from the *LP* GRS observations (Lawrence et al. 2000; Prettyman et al. 2006), the *CE-2* Th map shows a slightly different percentage distribution in the FHT. In the lunar highlands, most areas have Th concentration of ~ 1.2 ppm, comparable to ~ 1.4 ppm (Lawrence et al. 2000) and ~ 0.8 ppm (Prettyman et al. 2006) for the *LP* GRS Th data. However, this value is still on an order of three times higher than the average Th estimation (0.37 ± 0.11 ppm) of the FHT derived from feldspathic lunar breccias (Korotev et al. 2003). Although the average Th estimation from lunar breccias is always used to represent a potential Th abundance for the feldspathic crust unmodified by Th-bearing mare basalts or Th-rich Imbrium ejecta, most of the lunar surface ($\sim 97\%$) has a Th concentration larger than this value. The areas with low Th concentration are likely averaged out in constructing the profiles by the surrounding areas with the higher Th value.

2.3 The Thorium Distribution with the Distance from Imbrium Basin

The fact that all the high-Th regions within the PKT are localized surrounding the Imbrium basin gives rise to an assumption that all the Th on the lunar surface including the farside highlands directly resulted from the ejecta of Imbrium basin (Haskin 1997). Haskin (1998) estimated the ejecta distribution from the Imbrium impact event by using the scaling relationships (Housen et al. 1983) and found that its ejecta spread globally covering the entire lunar surface. In addition, the agreement of the Th concentration with the GRS observations from the Apollo (Metzger et al. 1977) and *LP* (Lawrence et al. 1998) spacecraft strengthened this assumption.

The crust at the Imbrium target is generally rigid (Ferrari et al. 1978; Solomon & Head 1980) and enriched in thorium and other incompatible elements before the impact event (Haskin 1998; Jolliff et al. 2000), as a con-

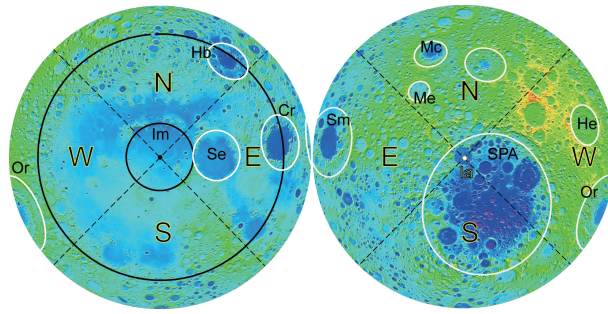


Fig. 5 The nearside and farside topographies of the Moon display the quadrants in this study (N, E, S, W – northern, eastern, southern and western quadrants respectively). The *inner black line* on the nearside represents the topographic ring of Imbrium basin (Im). The *outer one* outlines the boundary of mare basalts on the nearside. The *white line* on the farside represents the boundary of SPA basin. The *white circles* represent large basins on the lunar highlands surface as listed in Table 1. Abbreviations are: Cr, Crisium basin; Mc, Moscoviense basin; Me, Mendeleev basin; Se, Serenitatis basin; Hb, Humboldtianum basin; Sm, Smythii basin; He, Hertzprung basin; Or, Orientale basin; Im, Imbrium basin; la, Imbrium antipode.

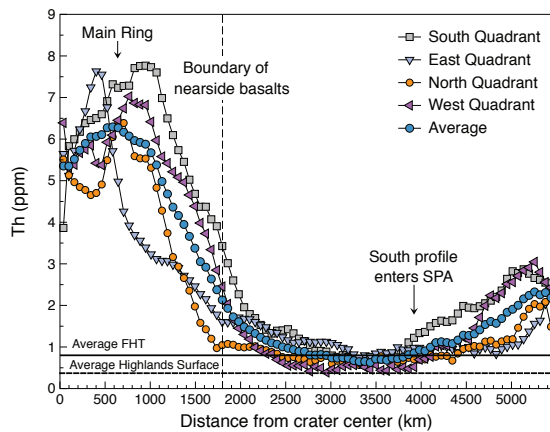


Fig. 6 The Th profile for each quadrant as well as the average Th profile for 360° around Imbrium basin versus distance from the center of the Imbrium basin. The *bold line* with value of 0.37 ppm and the *dashed line* with value of 0.80 ppm represent the estimated average Th concentration of the FHT defined by Korotev et al. (2003) and Jolliff et al. (2000), respectively.

sequence, the ejecta should be enriched in Th as well. This assumption has already been supported by the high-Th regions around the Imbrium basin in the PKT. Due to the high-Th ejecta spread globally over the lunar surface (Haskin 1998), thorium from the Imbrium basin is considered to be significant. Nevertheless, a key question remains as to how much of the Th on the lunar highlands originated from the Imbrium impact event? Are there any other contributions? In an attempt to address these issues, we focus on investigating the symmetry of the Th profiles radiating from the center of Imbrium basin at first. Assuming a vertical impact formed Imbrium basin, the ejecta are thought to be symmetric and possess a symmetric Th distribution. Therefore, assessment of the symmetry of Th distribution around Imbrium basin can constrain whether the Imbrium impact event is the only contributor to Th on the lunar surface.

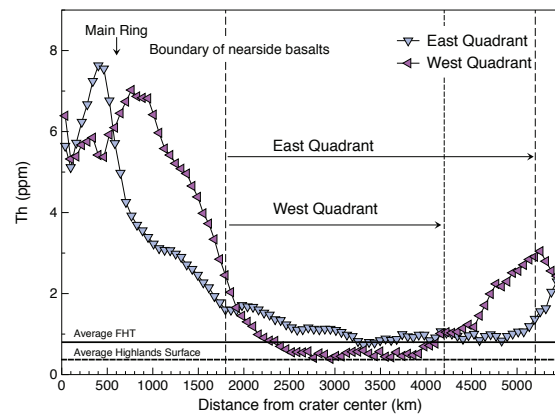


Fig. 7 The Th profile for the eastern and western quadrants versus distance from the center of the Imbrium basin. The transition from near-field to middle-field is at a distance of ~ 1800 km from the Imbrium center. The *bold line* with value of 0.37 ppm and the *dashed line* with the value of 0.80 ppm represent the estimated average Th concentration of the FHT defined by Korotev et al. (2003) and Jolliff et al. (2000), respectively.

To assess the variation in Th abundance around Imbrium basin, we follow the work of Petro & Pieters (2006a) and divide the lunar surface into four 90° quadrants centered on Imbrium and keep each quadrant containing the extent of unique areas within 90° of the basin. These four equally sized quadrants around the center of Imbrium basin are as shown in Figure 5, on which the inner black line on the nearside represents Imbrium topographic ring and the outer one corresponds to the boundary of mare basalts. The average Th profile for each quadrant as well as the average Th profile for 360° around Imbrium is illustrated in Figure 6. All the Th profiles, including the average Th profile, display similar patterns with the highest Th abundances close to the Imbrium topographic rim. However, outwards from the rim, the Th abundance steeply decreases and then keeps a stable value between 0.5–1.2 ppm. At large distances (~ 4000 km) from

the basin, the Th abundances begin to increase again to values of ~ 3.0 ppm. From profiles of the Th distribution, Petro & Pieters (2006a) defined three distinct regions along the distance from the Imbrium center: the near-field with the decrease in Th outside the Imbrium topographic rim to the boundary of mare basalts on the nearside, middle-field covering the area between ~ 2000 km and 4000 km where Th values are at a minimum, and the far-field covering distances greater than ~ 4000 km where Th values increase towards the antipode.

2.3.1 Asymmetric thorium distribution around the Imbrium basin

In the near-field, the high Th is mainly associated with the Imbrium topographic ring. At the Imbrium topographic ring, the average Th abundance is ~ 6.5 ppm for the western, eastern and northern quadrants (Fig. 6). However, the average value is a little high for the southern quadrant (~ 7.5 ppm). This high Th value is mainly associated with the Fra Mauro Highlands, the largest continuous region of elevated thorium over the Moon (Jolliff et al. 2000). The high Th value forms a peak at each profile. In contrast with the northern and southern quadrants where the Th peak occurs at the topographic ring of Imbrium basin, the highest Th value for the eastern and western quadrants occurs a little further away (see Fig. 6). This is mainly due to small area Th features, which have particularly higher Th concentration than the background and strongly affect the average Th profile. For example, the Th peak for the western quadrant occurs at 200 km further than the main ring of the Imbrium basin, corresponding to the high Th crater Marian. The highest Th value for the eastern quadrant occurring at the inner part of the Imbrium ring is associated with the crater Aristillus, which is thought to excavate high-Th materials from the floor of Imbrium basin (Lawrence et al. 2003). If we neglect the effect of these small-area Th features and assume that the Th enhancement in the Fra Mauro region is only a partial result of Imbrium ejecta, the Th profiles in Figure 6 suggest a symmetric distribution of Th (~ 6.5 ppm) at the ring of Imbrium basin.

Each Th profile decreases with the distance outwards from the Imbrium basin to the mare basalt boundary of the nearside, however, the Th value in the near-field is likely not due to the presence of Imbrium ejecta. These are mainly associated with mare basalts or pre-existing high Th formation around the Imbrium basin (see Fig. 5) (Haskin et al. 2000). For example, the Th value of the northern quadrant is mainly associated with Mare Frigoris located ~ 1000 km from the Imbrium center and that of the western quadrant is associated with western Oceanus

Procellarum, both of which are enriched in radioactive elements in the PKT. The greatest Th variation identified in the eastern quadrant is mainly because of the presence of non-PKT mare basalts within Maria Serenitatis, Tranquillitatis and Nectaris, which subdues the average Th profile in the near-field (Jolliff et al. 2000). In the southern quadrant, the Th profile is enhanced at the Fra Mauro formation, in which the Th signature is thought to be only a portion of the Th signature from Imbrium ejecta (Haskin et al. 2000). Although the Th abundance at the topographic ring of Imbrium basin is symmetric, the difference in the Th peak position and the variation of Th profile of each quadrant indicate an asymmetric Th distribution around Imbrium basin in the near-field.

2.3.2 Symmetric thorium distribution on the lunar farside highlands

The average Th profile of each quadrant possesses unique features in the near-field, but presents a similar pattern in the middle-field (see Fig. 6). The transition from near-field to middle-field occurs at the distance of ~ 1700 to 2000 km from the Imbrium center, beyond which the Th abundance remains a stable value between 0.5 ppm and 1.2 ppm. For example, the Th profile keeps an average value of 0.5 ppm at the distance of ~ 2200 to 4000 km from the Imbrium center for the western quadrant and 1.0 ppm at the distance of 1800 to 4200 km for the northern quadrant. The Th abundance decreases to ~ 1.5 ppm occurring at ~ 2300 km from the Imbrium center for the southern quadrant, a little further than those of western and northern quadrants. It is due to the high-Th Fra Mauro formation extending a little part in the middle-field. However, once the profile enters the farside highlands, the Th profile shows a low Th abundance, much like the other quadrants. The Th profile of the eastern quadrant remains above the values of the western quadrant through the middle-field (see Fig. 7). In contrast with the asymmetric Th distribution in the near-field, the Th profiles in the middle-field have a symmetrical distribution around the center of Imbrium basin. The Th abundances in the near-field are associated with mare basalts or pre-existing high Th formation, unrelated to Imbrium ejecta. Nevertheless, the distinct transition between the near-field and middle-field indicates a separate process of Th distribution in the middle-field, which might be related to Imbrium ejecta.

All the profiles in the middle-field exhibit a Th concentration on an order of 2 or 3 times greater than the estimated highlands value of 0.37 ± 0.11 ppm derived from lunar meteorites (Korotev et al. 2003) but are consistent with the estimated FHT value of 0.8 ± 0.3 ppm from the $LP 5^\circ \times 5^\circ$ Th map (Jolliff et al. 2000). The estimated Th abundance from

lunar meteorite data is thought to represent the average Th abundance for the feldspathic crust. Nevertheless, these low Th abundances are likely averaged out in constructing the profiles by the higher average Th value because of only a very low percentage of the lunar surface having abundances less than 0.37 ppm (see Fig. 4). The average Th abundance greater than the estimated value in the middle-field implies other sources for the Th in the middle-field, much like from the Imbrium ejecta. However, the question on how much of the Th in the middle-field originated from the Imbrium impact event still remains unanswered. Besides the Imbrium ejecta, are there any other contributors? Although the Th distribution on the middle-field is symmetric around the Imbrium basin, we still cannot answer this question now. In order to address these issues, we use an impact model based on the impact scaling-laws to estimate the thorium concentration on the lunar highlands contributed by the Imbrium ejecta in the following section.

2.4 The Modeled Thorium on the Lunar Highlands Surface from Imbrium Basin

The Imbrium basin, formed about 3.85 billion years ago (Stöffler & Ryder 2001), is one of the youngest basins on the Moon. The Imbrium basin is ~ 1160 km in diameter (Spudis 1993) and its transient crater is ~ 375 km in radius (Wieczorek & Phillips 2000) (see Table 1). Here we assume that the crust of the target was homogenous in thorium (Spudis et al. 1988) before the Imbrium impact. According to the symmetric thorium distributions at the Imbrium topographic ring and in the middle-field, we assume that the Imbrium event is a vertical impact event in our model and the ejected thorium abundance on the lunar highlands is associated with the ejecta thickness derived from the Imbrium basin.

2.4.1 The modeled ejecta thickness of Imbrium basin

The ejecta thickness from the Imbrium basin can be estimated based on the scaling equation (Housen et al. 1983) in a constant gravity regime

$$\frac{t}{R_0} = \frac{A(e_r - 2)}{2\pi} (\sin 2\theta)^{e_r - 2} \left(\frac{R}{R_0}\right)^{-e_r} \times \left[1 + \frac{4e_r - 5}{3} \left(\frac{R/R_0}{\sin 2\theta}\right)^{-(e_r - 2)/2} \frac{0.62^{1/e_x}}{R/R_0}\right]. \quad (1)$$

Here, t is the ejecta thickness of the Imbrium basin; R_0 is the transient crater radius of the Imbrium basin (~ 375 km); R is the radial distance from the Imbrium center; A is a constant (0.20) in the gravity regime (Stoeffler et al. 1975); θ is the ejecta launch angle related to the lunar surface (45°); e_r and e_x are crater scaling exponents with a value of 2.61 and 1.81, respectively (Housen et al. 1983).

The ejecta thickness variation along with radial distance from the Imbrium center is shown in Figure 8(a), from which the ejecta thickness decreases with the increasing distance at first, then goes through a minimum, and finally reaches a peak at the antipode of Imbrium basin. The ejecta thickness is about 6.50 km at the rim of transient crater (~ 375 km) and 4.20 km at the rim of the basin (~ 600 km). The estimated ejecta thickness at the rim of Imbrium basin is reasonable in comparison with the ejecta thickness of ~ 3.0 km at the rim of Orientale basin with a diameter of 960 km (Fassett et al. 2011; Zhu et al. 2017). On the lunar farside highlands corresponding to the distance of Imbrium basin from ~ 1800 km to 4000 km, the ejecta thickness varies from ~ 80 m to ~ 50 m. However, on the antipode of Imbrium basin, the thickness reaches ~ 200 m.

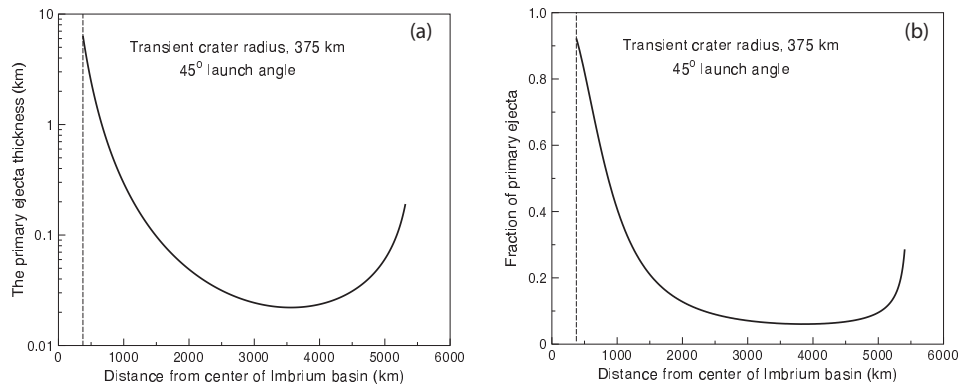
We calculate all the primary ejecta fragments and their secondary excavated materials while falling back to the lunar surface. We assume that the size distribution of the primary fragment follows the power law size distribution $N(\geq m) = Cm^{-b}$. Here, $N(\geq m)$ represents the total number of primary ejecta fragments with masses equal to or greater than m . Note, the mass of the largest fragment (m_f) is considered to be a function of total mass of the ejecta (M): $m_f = 0.8M^{0.8}$, here $M = \pi\rho(2R_0)^3/80$ if we assume that the excavation cavity is parabolic with a depth-diameter ratio of 0.1 (Melosh 1989). The size of primary fragments ranges from 10^{-6} g (impact-produced dust) to m_f (largest fragment). With these assumptions, we use the π -group scaling relationships (Housen et al. 1983) to calculate the size distribution of the secondary craters produced by the primary fragments re-impacting on the lunar surface. The mixing of the primary fragments and the excavated substrate materials is assumed to be uniform (see Haskin 1998; Haskin et al. 2003). As a consequence, the amount of primary ejecta is the mass ratio between the primary fragment and total material, consisting of the primary ejecta and local material excavated by the primary ejecta. Assuming that the primary fragments derived from the Imbrium basin are enriched in thorium, the proportion of primary fragments in the total material, as shown in Figure 8(b), can indicate the thorium amount originating from the Imbrium impact event (Haskin et al. 2003).

It can be found that the proportion variation is different from the deposit thickness. It decreases rapidly from 92% at the Imbrium rim to 17% at a distance of 1800 km. A high proportion of primary ejecta fragments located in the Imbrium rim is mainly due to a large amount of primary ejecta falling back here (Zhu et al. 2017) and a very small amount of substrate is excavated because of low velocities. The proportion curve keeps a minimum value (from 15% to 8%) within the distance from 1800 km to 4000 km in

Table 1 The locations, diameters, impact depth and crust thicknesses of Imbrium and other related basins. The basins are listed in stratigraphic order with the oldest basin at the top and youngest basin at the bottom (Wilhelms et al. 1987).

Basin	Location ^a (Lat, Lon)	Main Ring Diameter ^b (km)	Impact Depth ^c (km)	Crustal Thickness ^d (km)
Smythii	(−2°, 87°)	740	44.3	5.7
Freundlich-Sharonov	(18.5°, 175°)	600	33.0	13.5
Moscoviense	(26°, 147°)	420	18.9	0.6
Korolev	(−4.5°, −157°)	440	20.5	44
Humboldtianum	(61°, 84°)	650	33.1	0.3
Crisium	(17.5°, 58.5°)	740	48.7	3.1
Serenitatis	(27°, 19°)	920	65.7	6.7
Hertzprung	(1.5°, −128.5°)	570	30.7	19.5
Imbrium	(33°, −18°)	1160	74.4	9.8
Oriente	(−20°, −95°)	930	39.7	6.5

^a Wilhelms et al. (1987); ^b Spudis (1993); ^c $\sim 0.1 \times$ transient crater diameter; the transient crater diameters are from Petro & Pieters (2008) and Wieczorek & Phillips (1997); ^d Wieczorek et al. (2013).

**Fig. 8** (a) The modeled thickness of ejecta deposits from Imbrium basin versus distance from the center of Imbrium basin; (b) The fraction of Imbrium primary ejecta on the lunar surface as a function of distance from the Imbrium center. The radius of Imbrium transient crater is assumed to be 375 km (Wieczorek & Phillips 2000) and all the ejecta is assumed to be launched with an angle of 45°.

areas corresponding to the lunar highlands. But the value increases beyond the distance of 4000 km and reaches a high value at the antipode of Imbrium basin because of the focusing effect of the ejecta.

Although the primary fragment size distribution, the launching angles and the characteristics of substrate material would affect the proportion of primary fragment in the calculation, these parameters do not significantly affect the simulation results when considering the real impact event that forms a large-scale structure like the size of Imbrium basin (Haskin et al. 2003). For example, laboratory impact experiments indicate that the launch angles of most primary fragments range from 35° to 55° (Cintala et al. 1999). However, the estimated ejecta thicknesses by using an average launch angle of 45° for all the primary fragments have no significant variations for the real observations (Stoeffler et al. 1975) and the hydrocode simulations (Zhu & Wunnemann 2013; Zhu et al. 2015; Zhu et al. 2017). Therefore, we use this proportion curve to investi-

gate the modeled Th contribution by the Imbrium basin on the lunar farside highlands in the following section.

2.4.2 The modeled thorium concentration on the lunar surface

Since the crust was assumed to be rigid and homogeneous in radioactive elements before the Imbrium-forming impact event, the primary fragments from Imbrium basin are therefore enriched in Th and the proportion of primary fragments in the total ejecta deposits as shown in Figure 8(b) indicates that the Th amount originated from Imbrium basin. Given the proportion of primary fragments in the ejecta deposits, the average Th concentration of these deposits at any distance from Imbrium basin can be estimated if the Th concentrations of Imbrium primary fragment and preexisting substrate are known. Previously, Haskin (1998) used the average Th concentration of the Imbrium ejecta (~ 5 ppm) and the preexisting substrate (~ 0.1 ppm) as the “ground-truth” values for calibration

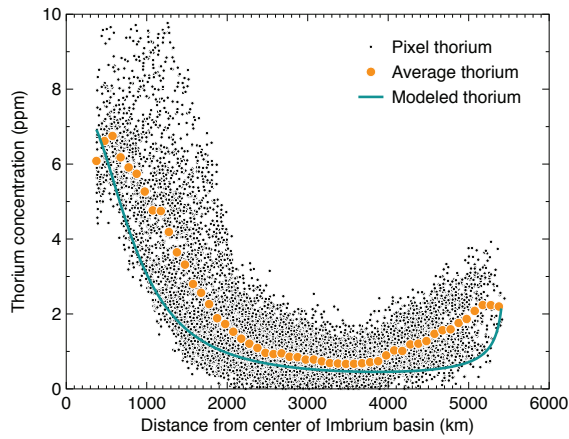


Fig. 9 The Th distribution outside the Imbrium rim versus distance from the center of the Imbrium basin. The *black points* are the pixel Th concentrations (60 km \times 60 km) and the *orange solid points* are the average Th abundances in the concentric anchor rings from 375 km to the Imbrium antipode with an increment of 100 km. The *line* represents the modeled Th using the scaling-laws.

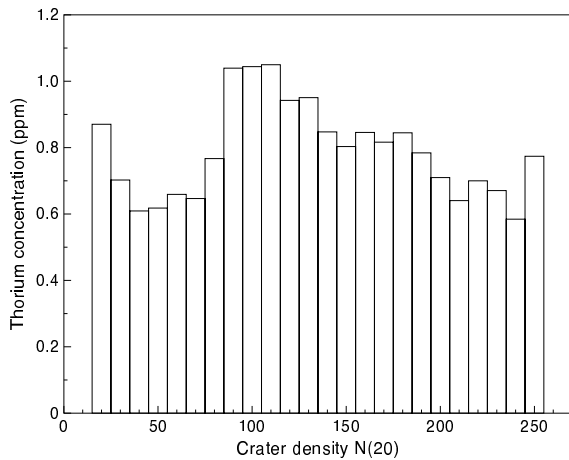


Fig. 10 The relation of Th with crater density on the lunar highland surface. All the Th and crater density maps are rebinned into $5^\circ \times 5^\circ$ pixels. The crater density data are from Head et al. (2010) in which craters with diameters larger than 20 km are considered.

of the percentage curve in Figure 8(b). However, since most lunar surface experienced a saturated impact history after Orientale basin (~ 3.8 Ga, see Head et al. 2010) that changed the original Th concentration of the preexisting substrate, the Th values of the Imbrium ejecta on the lunar highlands surface were mostly mixed or contaminated by subsequent heavy impacts (Huang et al. 2017). Furthermore, Haskin (1998) used the Th concentrations from the observations of Apollo GRS, from which the selected Th value of ~ 5 ppm as the “ground-truth” value may not correctly represent the concentration of Imbrium ejecta and 0.1 ppm was a little lower than the average estimation for the preexisting substrate (Korotev et al. 2003).

Here, we select the average Th concentrations from the Imbrium rim (uncovered by subsequent mare activities) and four craters, Aristarchus (25°N , 48°W), Mairan (41°N , 43°W), Aristillus (33°N , 3°E), and Kepler (7°N , 38°W) (see Fig. 3) to calibrate the percentage curve for the modeled Th on the lunar surface. We list the reasons as follows:

(1) The rim of Imbrium basin (uncovered by the subsequent mare activities) was excavated from the impact target during the impact cratering process and its Th abundance could represent the value in the pre-impact target;

(2) The craters Aristarchus, Mairan, Aristillus and Kepler are located close to the Imbrium rim. These four craters were created after the formation of Imbrium basin. When these basins were formed, the impactors penetrated through the mare basalts and excavated the materials of Imbrium ejecta beneath the mare basalts. These four craters have symmetric Th distributions around Imbrium basin ($\sim 8 - 10$ ppm; Mairan $\sim 7.5 - 9$ ppm; Aristillus $\sim 7 - 9$ ppm, Kepler $\sim 7 - 9$ ppm) and, therefore, the Th values from these four craters can represent the Th abundance from the Imbrium ejecta at their locations;

(3) The Imbrium rim (uncovered by subsequent mare activities) and four craters are far away from Orientale basin, the only large basin younger than Imbrium basin. These areas were not contaminated by the Orientale ejecta or other geologic activities (Lawrence et al. 2000), and therefore could correctly represent the initial Th values excavated by the Imbrium impact event.

The average Th value of 6.5 ppm derived from these areas is used as the “ground-truth” of the Imbrium ejecta in our calibration. It should be noted that other high-Th regions are excluded mainly because they might have heavy contaminations from the ejecta of surrounding impacts or volcanism. For example, the high-Th region around Apennine Bench ($25^\circ - 28^\circ\text{N}$, $0^\circ - 10^\circ\text{W}$) in the southeast of Imbrium basin is excluded because it was possibly flooded by post-Imbrium KREEP basalt (Spudis 1978). For the value of preexisting substrate, we use the average estimation of 0.37 ± 0.11 ppm derived from 11 feldspathic lunar breccias (Korotev et al. 2003). This value is thought to represent a potential Th abundance for the feldspathic crust unmodified by Th-bearing mare basalts or Th-rich Imbrium ejecta (Korotev et al. 2003) and therefore could be regarded as a “ground-truth” point for the Th abundance of preexisting substrate in the middle-field.

The calibrated line, as shown in Figure 9, displays the modeled Th concentration within a distance from the Imbrium transient crater rim to its antipode. The area with the highest Th concentration of ~ 6.0 ppm is located at the Imbrium rim, then the concentration decreases with increasing distance. The areas with the low Th concentration

of ~ 0.7 ppm appear within the distance of 1800 km to 4000 km corresponding to the lunar farside highlands, then the Th concentration increases until the Imbrium antipode and arrives at ~ 2.1 ppm at SPA, in agreement with the observation. Although the modeled Th concentration around the rim of Imbrium basin is consistent with the observed value, the modeled value on the farside highlands is only 60% to 70% of the observations.

In modeling, we assume that the target crust was rigid and homogeneous in composition before the Imbrium impact. The rigid lithosphere implies that the Moon might have finished its compositional fractionation and differentiation processes from the magma ocean and the anorthositic crust, KREEP materials and mantle would have been already layered. Since the radioactive elements do not readily substitute the elements in the crystal lattices of dense mantle and light crustal minerals in the early crystallization (Korotev 1998), the Th concentration in the lunar crust should be lower than the homogeneous value assumed in this study. This assumption results in an overestimation of the Th value on the lunar highlands contributed by Imbrium basin. However, these overestimated values should represent an upper limit of the Th contribution by Imbrium basin on the lunar highlands surface. Nevertheless, the fact that the upper limit of the predicted value is lower than the observations implies a relatively small contribution from Imbrium basin for the Th on the lunar highlands. If we consider the real case in our model, e.g., the low-Th feldspathic crust, the varied launch angles of the primary ejecta fragments and the effect of the mixture between primary fragment and substrate, the Th concentration on the lunar highlands contributed by Imbrium basin is reduced by about half. A rough estimation of 20%–30% is suggested based on our model. This rough estimation is consistent with the proportion of the impact melt-breccia component derived from Imbrium basin (15%–23%) in the Apollo 16 regolith (Korotev 1997; Petro & Pieters 2006b).

2.5 Do the Highlands Have a High Thorium Concentration Before the Imbrium Basin-forming Impact?

The Imbrium impact penetrated through the lunar crust to the mantle and excavated voluminous KREEP materials (Yamamoto et al. 2010), however, its ejecta thickness is only $\sim 30 - 50$ m beyond ~ 1800 km from the Imbrium center and, therefore, has a very small Th contribution on the highlands. Similar estimations of other large basins, such as Serenitatis ($D \sim 920$ km), Crisium ($D \sim 740$ km) and Orientale ($D \sim 930$ km), suggest a negligible effect of these basins due to the low-Th concentration in the rim and

surrounding ejecta blanket for each basin (Petro & Pieters 2008). Jutzi & Asphaug (2011) hypothesized that the accretion of a companion moon could form the lunar farside highlands and simultaneously push the KREEP-rich layer on the farside to the nearside. However, the inexplicable relations of the Th concentrations to the topography (Lawrence et al. 2000) and crustal thickness (Kobayashi et al. 2012) cast doubt on such an origin for the Th on the lunar highlands. Now, the questions are whether these exogenic materials are not responsible for the Th on the lunar highlands, and what is the significant contributor?

According to the crystallization process of the lunar magma ocean, the feldspar-rich crust was formed early (Norman et al. 2003). The subsequent long-term impacts result in a state of saturation equilibrium (Strom et al. 2005; Head et al. 2010) for craters with a size from several meters to several hundred kilometers on the lunar surface. The large impacts excavate voluminous deep materials to the lunar surface and mix with the local material. As a consequence, the surface materials on the most densely cratered area are uniformly mixed by the local material, the excavated material from the deep area and the low-Th impactor. If the local material on the surface of the highlands surface has a Th concentration lower than the value of Imbrium ejecta, the mixed material on the highlands has a lower Th concentration than the value of Imbrium ejecta because the pre-existing materials will dilute the Th value in the Imbrium ejecta during the mixing process. The subsequent impacts accrete low-Th impactor on the highlands, which increases the extent of mixture but decreases the Th concentration of the material on the highlands. However, the Th map observed by the CE-2 GRS has a relatively higher Th concentration than the theoretical value on the highlands (see Fig. 9). It implies that the higher Th material has probably existed on the highlands before the formation of the Imbrium basin. The mixture of the Imbrium ejecta with the local material on the lunar surface dilutes the Th concentration.

Assuming all the large basins on the Moon have made negligible contributions, the current Th distribution on the highlands is the end product resulting from the impact cratering process from its initial stage to current status. The relation with crater density would display its variation on the lunar highlands. We re-bin all the craters on the lunar highlands with diameter greater than 20 km into $5^\circ \times 5^\circ$ pixels according to their central locations (Head et al. 2010). The relation of the Th concentration with the crater density is shown in Figure 10, from which the Th values are found to keep a very small variation (from 0.8 ppm to 1.1 ppm) no matter the variation of the crater density. This small Th variation with crater density suggests that the Th materials on the highlands have existed for a long time.

Further, the craters on the lunar highlands have sizes ranging up to several hundred kilometers. These craters excavate deep crustal materials mixing with the substrate surface. However, no clear variation of the Th concentrations in the mixed materials appearing with the depths of excavation is found on the lunar highlands. All of these indirectly imply that the local Th has existed on the lunar highlands surface before the Imbrium basin-forming impact.

The native Th on the highlands is a complicated product by the formation of plagioclase crust (Warren 1985; Snyder & Taylor 1993; Kobayashi et al. 2012) and the modifications of heavy impact processes. Although the radioactive elements K, Th and U are not readily included into the crystal structure of the minerals in the early crystallization of the lunar magma ocean (Korotev 1998), the KREEP was entrained during the formation of the plagioclase crust (Kobayashi et al. 2012), in which the Th concentration gradually increased with an increase of depth (Snyder & Taylor 1993). The top layer of the plagioclase crust, which was initially formed, has no Th composition. However, the subsequently heavy impacts excavated voluminous deep and a relatively high-Th material to the lunar surface and then mixed with the local materials. With the long-term impacts, the top layer of lunar crust was overturned and uniformly mixed with the deep material. As a consequence, the Th concentration on the lunar surface increased with time and eventually reached a constant value as we observed on the highlands when the lunar surface reached a saturated impact state.

2.6 The Difference in Average Thorium Concentration Between the Eastern- and Western-Farside Highlands

The difference in average Th concentration between the eastern- and western-farside highlands of the Moon was discovered in previous studies (e.g., Metzger et al. 1977; Kobayashi et al. 2012). This difference was confirmed by the new Th map (see Fig. 2 and Fig. 7), from which the average Th concentration in the eastern farside highlands is ~ 1.1 ppm and a little higher than the value (~ 0.7 ppm) in the western regions. However, the Th concentration in the western-highlands has a more uniform distribution than that in the eastern portion.

This difference in the Th concentration between the eastern- and western-highlands of the Moon was linked to variations in the crustal thickness, in which a striking inverse relation between the thorium concentration and crustal thickness was indicated in previous studies (Metzger et al. 1977; Trombka et al. 1973; Metzger 1993; Lawrence et al. 2000; Kobayashi et al. 2012). That is, the highlands with a thicker crust have lower Th concentration

whereas those with a thinner crust have a higher Th value. According to the inverse relationship, Metzger (1993) proposed that the current Th on the lunar highlands is representative of the underlying crust because its initial characteristic of highlands surface is not destroyed by the lateral and vertical mixing due to bombardment. Kobayashi et al. (2012) suggested that the lateral inhomogeneous crystallization of the lunar magma ocean owing to tidal heating (Garrick-Bethell et al. 2010) is responsible for the Th difference in the eastern- and western-highlands of the Moon. In light of the time difference related to the crust formation, the crust that is crystallized earliest from the lunar magma ocean is thicker and has the lowest Th abundance and vice versa (Kobayashi et al. 2012). However, recent study indicates that several large-scale impact basins might penetrate through the crustal thickness and excavate materials from the lower crust or the upper mantle onto the lunar surface (Fig. 11) (Wieczorek et al. 2013), which might control the Th difference in the lunar highlands surface. The hypothesis of lunar magma ocean suggests that the Th concentration increases gradually with the depth of crustal thickness in its initial state (Snyder & Taylor 1993). Thus, the impact events on the thin crust would make it easier to excavate deep materials with a relatively high Th concentration than those on the thick one. The new crustal map derived from the *Gravity Recovery and Interior Laboratory (GRAIL)* mission (Fig. 11) indicates that the thicknesses of most western highlands range from ~ 40 km to ~ 60 km whereas in the east the thickest crust is ~ 40 km (Wieczorek et al. 2013). Therefore, it is easier for the cratering-formation events on the eastern highlands to excavate high-Th materials than those on the western highlands. For example, the Moscoviense basin ($D \sim 420$ km) on the eastern highlands has a comparable diameter with the Korolev basin ($D \sim 440$ km) on the west, however, the former basin was thought to penetrate through the crust whereas the later one only excavated the upper crustal materials (see the values of excavation depth and crustal thickness in Table 1; the excavation depth is ~ 0.1 of the diameter of a transient crater, Melosh 1989).

Additionally, there are several large impact events on or near the eastern highlands regions (e.g., Moscoviense, Crisium, Smythii and Humboldtianum, see Table 1 and Fig. 11) that penetrated through the crustal thickness into the mantle (Yamamoto et al. 2010). Their voluminous ejecta enriched the high-Th materials and covered the entire eastern region which resulted in the increase of Th concentrations on the highlands surface while mixing with the initial low-Th substrate. Although there are also several large basins on the western-highlands of the Moon (e.g., Orientale ($D \sim 930$ km), Hertzprung ($D \sim 570$ km) and Korolev ($D \sim 440$ km), see Table 1 and Fig. 11), they did

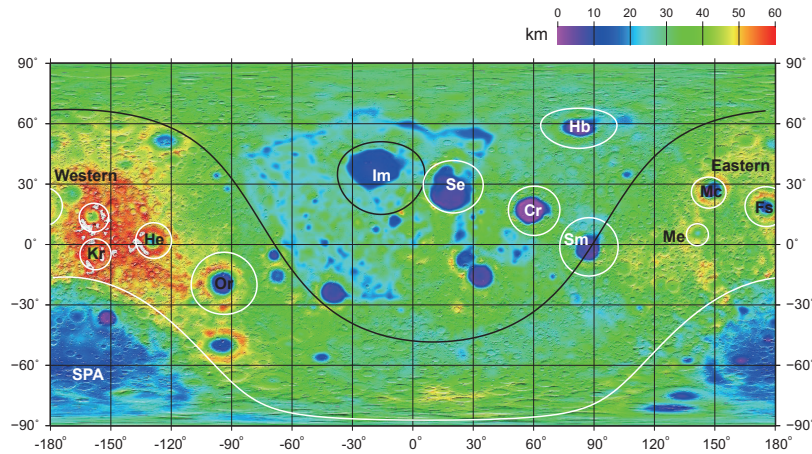


Fig. 11 The crustal thickness derived from *GRAIL* observation (Wieczorek et al. 2013). The *black line* on the nearside represents the topographic ring of Imbrium basin (Im); the *outer black one* outlines the boundary of mare basalts on the nearside; The *white line* on the farside indicates the boundary of SPA basin. The *white circles* signify large basins on the lunar highlands surface as listed in Table 1. Abbreviations are: Cr, Crisium basin; Mc, Moscoviense basin; Me, Mendeleev basin; Se, Serenitatis basin; Hb, Humboldtianum basin; Sm, Smythii basin; He, Hertzprung basin; Or, Orientale basin; Im, Imbrium basin.

not penetrate through the thicker crust and excavate deep high-Th materials or only excavate a little high-Th materials (e.g., Orientale basin, Zhu et al. 2013, 2015).

3 CONCLUSIONS

In this paper, we present the global thorium map derived from observations by *CE-2* GRS. This new map shows a thorium distribution that is consistent with previous observations (e.g., *LP*, *Kaguya* and *Chang'E-1*), in which the PKT has a thorium concentration greater than 3 ppm, the SPAT has a concentration within the range between 1.5 ppm and 3.5 ppm, and the FHT has an average value smaller than ~ 1.5 ppm.

The Th on the lunar surface was previously suggested to originate from ejecta of Imbrium basin. However, the Th profiles along the distance of Imbrium basin exhibit an asymmetric distribution in the near-field but symmetric distribution in the middle-field. The asymmetric distribution in the near-field is mainly associated with mare basalts or pre-existing high-Th materials, and not related to the Imbrium ejecta. In the middle-field, our impact model based on the scaling-laws indicates that the ejecta of Imbrium only contributes a small portion ($\sim 20\%$ – 30%) of Th abundance. Most Th in the middle-field might be indigenous which results from the mixtures of voluminous high-Th materials excavated from deep crust by native impact cratering processes and local low-Th substrate. The long-term impacts result in uniform mixing and constant Th concentration in the upper crust. The Th difference between the eastern- and western-highlands is also found in the new Th map. The thin crust and large basins over the

eastern highlands are responsible for the relatively higher Th concentration than that over the western-highlands of the Moon.

Acknowledgements We thank Noah Petro for his valuable comments on the early version of this manuscript and for providing us his unpublished work. Acknowledgements also go to the anonymous reviewer and Wing-Huen Ip for the insightful comments that improved this work. This work was supported by the National Natural Science Foundation of China (11773087) and the Science and Technology Development Fund of Macau (079/2018/A2).

References

- Cintala, M. J., Berthoud, L., & Hörz, F. 1999, *Meteoritics and Planetary Science*, 34, 605
- Fassett, C. I., Head, J. W., Smith, D. E., Zuber, M. T., & Neumann, G. A. 2011, *Geophys. Res. Lett.*, 38, L17201
- Feldman, W. C., Barraclough, B. L., Fuller, K. R., et al. 1999, *Nuclear Instruments and Methods in Physics Research A*, 422, 562
- Ferrari, A. J., Nelson, D. L., Sjogren, W. L., & Phillips, R. J. 1978, *J. Geophys. Res.*, 83, 2863
- Garrick-Bethell, I., & Zuber, M. T. 2009, *Icarus*, 204, 399
- Garrick-Bethell, I., Nimmo, F., & Wieczorek, M. A. 2010, *Science*, 330, 949
- Hasebe, N., Shibamura, E., Miyachi, T., et al. 2008, *Earth, Planets, and Space*, 60, 299
- Haskin, L. A. 1997, in *Lunar and Planetary Science Conference*, 28, 519
- Haskin, L. A. 1998, *J. Geophys. Res.*, 103, 1679

- Haskin, L. A., Gillis, J. J., Korotev, R. L., & Jolliff, B. L. 2000, *J. Geophys. Res.*, 105, 20403
- Haskin, L. A., Moss, W. E., & McKinnon, W. B. 2003, *Meteoritics and Planetary Science*, 38, 13
- Head, J. W., Fassett, C. I., Kadish, S. J., et al. 2010, *Science*, 329, 1504
- Hess, P. C., & Parmentier, E. M. 2001, *J. Geophys. Res.*, 106, 28023
- Housen, K. R., Schmidt, R. M., & Holsapple, K. A. 1983, *J. Geophys. Res.*, 88, 2485
- Huang, Y.-H., Minton, D. A., Hirabayashi, M., et al. 2017, *Journal of Geophysical Research (Planets)*, 122, 1158
- Jolliff, B. L., Gillis, J. J., Haskin, L. A., Korotev, R. L., & Wieczorek, M. A. 2000, *J. Geophys. Res.*, 105, 4197
- Jolliff, B. L., Wiseman, S. A., Lawrence, S. J., et al. 2011, *Nature Geoscience*, 4, 566
- Jutzi, M., & Asphaug, E. 2011, *Nature*, 476, 69
- Kernan, W. J. 2006, *IEEE Transactions on Nuclear Science*, 53, 395
- Kobayashi, S., Hasebe, N., Shibamura, E., et al. 2010, *Space Sci. Rev.*, 154, 193
- Kobayashi, S., Karouji, Y., Morota, T., et al. 2012, *Earth and Planetary Science Letters*, 337, 10
- Korotev, R. L. 1997, Some Things We can Infer about the Moon from the Composition of the Apollo 16 Regolith, *Meteorit. Planet. Sci.* 32, 447
- Korotev, R. L. 1998, *J. Geophys. Res.*, 103, 1691
- Korotev, R. L., Jolliff, B. L., Zeigler, R. A., Gillis, J. J., & Haskin, L. A. 2003, *Geochim. Cosmochim. Acta*, 67, 4895
- Lawrence, D. J., Feldman, W. C., Barraclough, B. L., et al. 1998, *Science*, 281, 1484
- Lawrence, D. J., Feldman, W. C., Barraclough, B. L., et al. 2000, *J. Geophys. Res.*, 105, 20307
- Lawrence, D. J., Elphic, R. C., Feldman, W. C., et al. 2003, *Journal of Geophysical Research (Planets)*, 108, 5102
- Ma, T., Chang, J., Zhang, N., et al. 2008, *Advances in Space Research*, 42, 347
- Ma, T., Chang, J., Zhang, N., et al. 2013, *Acta Astronomica Sinica*, 54, 291
- Melosh, H. J. 1989, *Impact Cratering: A Geologic Process* (Oxford University Press)
- Metzger, A. E., Haines, E. L., Parker, R. E., & Radocinski, R. G. 1977, in *Lunar and Planetary Science Conference*, 8, ed. R. B. Merrill, 949
- Metzger, A. E. 1993, Composition of the Moon as Determined from Orbit by Gamma Ray Spectroscopy, Remote Geochemical Analysis: Elemental and Mineralogical Composition, eds: C. M. Pieters, & P. Englert (Cambridge Univ. Press), 341
- Norman, M. D., Borg, L. E., Nyquist, L. E., & Bogard, D. D. 2003, *Meteoritics and Planetary Science*, 38, 645
- Petro N. E. & Pieters C. M. 2006a, Assessment of Basin Ejecta Symmetry: the Imbrium Example, Chapter 3, PhD thesis, Brown University
- Petro, N. E., & Pieters, C. M. 2006b, *Journal of Geophysical Research (Planets)*, 111, E09005
- Petro, N. E., & Pieters, C. M. 2008, *Meteoritics and Planetary Science*, 43, 1517
- Prettyman, T. H., Hagerty, J. J., Elphic, R. C., et al. 2006, *Journal of Geophysical Research (Planets)*, 111, E12007
- Reedy, R. C., Arnold, J. R., & Trombka, J. I. 1973, *J. Geophys. Res.*, 78, 5847
- Snyder, G. A., & Taylor, L. A. 1993, *Antarctic Meteorite Research*, 6, 246
- Solomon, S. C., & Head, J. W. 1980, *Reviews of Geophysics and Space Physics*, 18, 107
- Spudis, P. D. 1978, in *Lunar and Planetary Science Conference*, 9, 3379
- Spudis, P. D., Hawke, B. R., & Lucey, P. G. 1988, in *Lunar and Planetary Science Conference*, 18, ed. G. Ryder, 155
- Spudis, P. D. 1993, *The Geology of Multi-ring Impact Basins* (Cambridge Univ. Press)
- Stoeffler, D., Gault, D. E., Wedekind, J., & Polkowski, G. 1975, *J. Geophys. Res.*, 80, 4062
- Stöffler, D., & Ryder, G. 2001, *Space Sci. Rev.*, 96, 9
- Strom, R. G., Malhotra, R., Ito, T., Yoshida, F., & Kring, D. A. 2005, *Science*, 309, 1847
- Thomson, B. J., Grosfils, E. B., Bussey, D. B. J., & Spudis, P. D. 2009, *Geophys. Res. Lett.*, 36, L12201
- Trombka, J. I., Arnold, J. R., Reedy, R. C., Peterson, L. E., & Metzger, A. E. 1973, in *Lunar and Planetary Science Conference*, 4, 2847
- Warren, P. H. 1985, *Annual Review of Earth and Planetary Sciences*, 13, 201
- Wasson, J. T., & Warren, P. H. 1980, *Icarus*, 44, 752
- Wieczorek, M. A., & Phillips, R. J. 1997, *J. Geophys. Res.*, 102, 10933
- Wieczorek, M. A., & Phillips, R. J. 2000, *J. Geophys. Res.*, 105, 20417
- Wieczorek, M. A., & Zuber, M. T. 2001, *J. Geophys. Res.*, 106, 27853
- Wieczorek, M. A., Neumann, G. A., Nimmo, F., et al. 2013, *Science*, 339, 671
- Wilhelms, D. E., McCauley, J. F., & Trask, N. J. 1987, *The Geologic History of the Moon* (Washington: U.S. G.P.O.; Denver, CO, U.S. Geological Survey)
- Yamamoto, S., Nakamura, R., Matsunaga, T., et al. 2010, *Nature Geoscience*, 3, 533
- Yamashita, N., Hasebe, N., Reedy, R. C., et al. 2010, *Geophys. Res. Lett.*, 37, L10201
- Zhu, M.-H., Ma, T., & Chang, J. 2010, *Planet. Space Sci.*, 58, 1547
- Zhu, M. H., & Wunnemann, K. 2013, in *Lunar and Planetary Science Conference*, 44, 1921
- Zhu, M.-H., Chang, J., Ma, T., et al. 2013, *Scientific Reports*, 3, 1611
- Zhu, M.-H., Wunnemann, K., & Potter, R. W. K. 2015, *Journal of Geophysical Research (Planets)*, 120, 2118
- Zhu, M.-H., Wunnemann, K., & Artemieva, N. 2017, *Geophys. Res. Lett.*, 44, 11